Simple merging technique for improving resolution in qualitative single image phase contrast tomography

Irvine, S ; Mokso, R ; Modregger, P ; Wang, Z ; Marone, F ; Stampanoni, M

DOI: https://doi.org/10.1364/OE.22.027257

Simple merging technique for improving resolution in qualitative single image phase contrast tomography

S Irvine,[1,2] R Mokso,[1] P Modregger,[1,2] Z Wang,[1] F Marone,[1] and M Stampanoni[1,3,*]

[1]*Swiss Light Source, Paul Scherrer Institut, 5232 Villigen PSI, Switzerland*
[2]*Centre d'Imagerie BioMedicale, Ecole Polytechnique Federale de Lausanne, 1015 Lausanne, Switzerland*
[3]*Institute for Biomedical Engineering, ETH Zurich, 8092 Zurich, Switzerland*
[*]*marco.stampanoni@psi.ch*

Abstract: For dynamic samples and/or for simple ease-of-use experiments, single-image phase contrast tomography is a very effective method for the 3D visualization of materials which would otherwise be indiscernible in attenuation based x-ray imaging. With binary samples (e.g. air-material) and monochromatic wavefields a transport-of-intensity (TIE)-based phase retrieval algorithm is known to retrieve accurate quantitative maps of the phase distribution. For mixed material samples and/or white beam radiation the algorithm can still produce useful qualitative tomographic reconstructions with significantly improved area contrast. The stability of the algorithm comes with a recognized associated loss of spatial resolution due to its essential behaviour as a low-pass filter. One possible answer to this is an image fusion technique that merges the slices reconstructed from raw phase contrast images and those after phase retrieval, where the improved contrast may be acquired without the associated loss of high-frequency information. We present this technique as a simple few-parameter Fourier method, which is easily tunable and highly compatible with current reconstruction steps.

OCIS codes: (340.7440) X-ray imaging; (100.5070) Phase retrieval; (100.6950) Tomographic image processing.

References and links

1. T. J. Davis, D. Gao, T. E. Gureyev, A. W. Stevenson, and S. W. Wilkins, "Phase-contrast imaging of weakly absorbing materials using hard X-rays," Nature **373**(6515), 595–598 (1995).
2. C. David, B. Nöhammer, H. H. Solak, and E. Ziegler, "Differential x-ray phase contrast imaging using a shearing interferometer," Appl. Phys. Lett. **81**(17), 3287–3289 (2002).
3. F. Pfeiffer, T. Weitkamp, O. Bunk, and C. David, "Phase retrieval and differential phase-contrast imaging with low-brilliance X-ray sources," Nat. Phys. **2**(4), 258–261 (2006).
4. T. Weitkamp, A. Diaz, C. David, F. Pfeiffer, M. Stampanoni, P. Cloetens, and E. Ziegler, "X-ray phase imaging with a grating interferometer," Opt. Express **13**(16), 6296–6304 (2005).
5. P. Cloetens, R. Barrett, J. Baruchel, J. P. Guigay, and M. Schlenker, "Phase objects in synchrotron radiation hard x-ray imaging," J. Phys. D Appl. Phys. **29**(1), 133–146 (1996).
6. A. Snigirev, I. Snigireva, V. Kohn, S. Kuznetsov, and I. Schelokov, "On the possibilities of x-ray phase contrast microimaging by coherent high-energy synchrotron radiation," Rev. Sci. Instrum. **66**(12), 5486–5492 (1995).
7. S. W. Wilkins, T. E. Gureyev, D. Gao, A. Pogany, and A. W. Stevenson, "Phase-contrast imaging using polychromatic hard X-rays," Nature **384**(6607), 335–338 (1996).
8. F. Pfeiffer, M. Bech, O. Bunk, P. Kraft, E. F. Eikenberry, Ch. Brönnimann, C. Grünzweig, and C. David, "Hard-X-ray dark-field imaging using a grating interferometer," Nat. Mater. **7**(2), 134–137 (2008).
9. D. M. Paganin, *Coherent X-ray Optics* (Oxford University, New York, 2006).
10. A. C. Kak and M. Slaney, *Principles of Computerized Tomographic Imaging* (IEEE, New York, 1999).
11. T. E. Gureyev, "Composite techniques for phase retrieval in the Fresnel region," Opt. Commun. **220**(1-3), 49–58 (2003).

#221629 - $15.00 USD Received 25 Aug 2014; revised 13 Oct 2014; accepted 14 Oct 2014; published 27 Oct 2014

12. M. R. Teague, "Deterministic phase retrieval—A Green's function solution," J. Opt. Soc. Am. **73**(11), 1434–1441 (1983).
13. D. Paganin, S. C. Mayo, T. E. Gureyev, P. R. Miller, and S. W. Wilkins, "Simultaneous phase and amplitude extraction from a single defocused image of a homogeneous object," J. Microsc. **206**(1), 33–40 (2002).
14. T. Weitkamp, D. Haas, D. Wegrzynek, and A. Rack, "ANKAphase: software for single-distance phase retrieval from inline X-ray phase-contrast radiographs," J. Synchrotron Radiat. **18**(4), 617–629 (2011).
15. W. S. Rasband, "ImageJ," *http://rsbweb.nih.gov/ij/* (2008).
16. M. A. Beltran, D. M. Paganin, K. Uesugi, and M. J. Kitchen, "2D and 3D X-ray phase retrieval of multi-material objects using a single defocus distance," Opt. Express **18**(7), 6423–6436 (2010).
17. M. A. Beltran, D. M. Paganin, K. K. W. Siu, A. Fouras, S. B. Hooper, D. H. Reser, and M. J. Kitchen, "Interface-specific x-ray phase retrieval tomography of complex biological organs," Phys. Med. Biol. **56**(23), 7353–7369 (2011).
18. T. E. Gureyev, A. W. Stevenson, Y. I. Nesterets, and S. W. Wilkins, "Image deblurring by means of defocus," Opt. Commun. **240**(1-3), 81–88 (2004).
19. E. Roessl, T. Koehler, U. van Stevendaal, G. Martens, N. Hauser, Z. Wang, and M. Stampanoni, "Image fusion algorithm for differential phase contrast imaging," Proc. SPIE **8313**, 831354 (2012).
20. Z. Wang, C. A. Clavijo, E. Roessl, U. V. Stevendaal, T. Koehler, N. Hauser, and M. Stampanoni, "Image fusion scheme for differential phase contrast mammography," J. Instrum. **8**(07), C07011 (2013).
21. R. C. Gonzalez and R. E. Woods, *Digital Image Processing* (Prentice Hall, 2008), pp. 954–954.
22. L. Turner, B. Dhal, J. Hayes, A. Mancuso, K. Nugent, D. Paterson, R. Scholten, C. Tran, and A. Peele, "X-ray phase imaging: Demonstration of extended conditions for homogeneous objects," Opt. Express **12**(13), 2960–2965 (2004).
23. P. Cloetens, M. Pateyron-Salomé, J. Y. Buffière, G. Peix, J. Baruchel, F. Peyrin, and M. Schlenker, "Observation of microstructure and damage in materials by phase sensitive radiography and tomography," J. Appl. Phys. **81**(9), 5878–5886 (1997).
24. M. Stampanoni, A. Groso, A. Isenegger, G. Mikuljan, Q. Chen, A. Bertrand, S. Henein, R. Betemps, U. Frommherz, P. Böhler, D. Meister, M. Lange, and R. Abela, "Trends in synchrotron-based tomographic imaging: the SLS experience," Proc. SPIE **6318**, 63180M (2006).
25. B. L. Henke, E. M. Gullikson, and J. C. Davis, "X-Ray Interactions: photoabsorption, scattering, transmission, and reflection at E = 50-30,000 eV, Z = 1-92," At. Data Nucl. Data Tables **54**(2), 181–342 (1993).
26. C. Hintermüller, F. Marone, A. Isenegger, and M. Stampanoni, "Image processing pipeline for synchrotron-radiation-based tomographic microscopy," J. Synchrotron Radiat. **17**(4), 550–559 (2010).
27. B. A. Dowd, G. H. Campbell, R. B. Marr, V. V. Nagarkar, S. V. Tipnis, L. Axe, and D. P. Siddons, "Developments in synchrotron x-ray computed microtomography at the National Synchrotron Light Source," in (International Society for Optics and Photonics, 1999), 224–236.
28. F. Marone and M. Stampanoni, "Regridding reconstruction algorithm for real-time tomographic imaging," J. Synchrotron Radiat. **19**(6), 1029–1037 (2012).
29. R. H. Huesman and G. T. Gullberg, "RECLBL library users manual—Donner algorithms for reconstruction tomography. Lawrence Berkeley Lab., Berkeley," (1977)
30. P. Modregger, D. Lübbert, P. Schäfer, and R. Köhler, "Two dimensional diffraction enhanced imaging algorithm," Appl. Phys. Lett. **90**(19), 193501 (2007).
31. G. Lovric, S. F. Barré, J. C. Schittny, M. Roth-Kleiner, M. Stampanoni, and R. Mokso, "Dose optimization approach to fast X-ray microtomography of the lung alveoli," J. Appl. Cryst. **46**(4), 856–860 (2013).
32. R. Mokso, F. Marone, S. Irvine, M. Nyvlt, D. Schwyn, K. Mader, G. K. Taylor, H. G. Krapp, M. Skeren, and M. Stampanoni, "Advantages of phase retrieval for fast x-ray tomographic microscopy," J. Phys. D Appl. Phys. **46**(49), 494004 (2013).

1. Introduction

The penetrative power of hard X-rays makes 3D tomography an excellent non-destructive technique for the micro- scale or even nano-scale characterization of samples, from biological and bio-medical applications to materials science and engineering. With high-flux sources, such as at a synchrotron facility, fast and *in situ* or *in vivo* scans of dynamic samples are increasingly utilized. In cases of materials with sufficient density variation, standard absorption contrast tomography may be sufficient, but for many light materials, the difference between the linear attenuation coefficient of various components leads to insufficient contrast from x-ray absorption alone. In these cases a form of phase contrast may be worthwhile- be it *e.g.* analyser-based [1] (also known as DEI, with a Bragg- or Laue-diffracting crystal), grating-based [2], [3] [4] (a form of differential phase contrast using at least one grating which is stepped across in sub-pixel distances) or propagation-based [5–7] (also known as in-line) phase contrast. Whilst the first two methods have their advantages in terms of sensitivity and multiple possible modes [4], [8], for sheer practicality and ease of use, propagation-based

#221629 - $15.00 USD Received 25 Aug 2014; revised 13 Oct 2014; accepted 14 Oct 2014; published 27 Oct 2014

imaging is ideal, requiring no extra optics, merely some distance between the sample and detector. Provided sufficient spatial coherence exists, this allows the phase modulations of the x-ray wavefield at the exit plane of the sample to propagate and self-interfere to be rendered as intensity modulations at the detection plane. Such ease of use means that the main experimental complexity, removed from the imaging step, can be reserved for the sample or experimental setup, e.g. dynamic, *in situ* arrangements.

In many cases, where the propagation-distance z is kept at a minimum and/or the spatial resolution and coherence is not so high, this effect is referred to as edge-enhancement and seen as an increase in the apparent sharpness of edges and voids within the sample. In simple radiographic projections, visibility of weakly or non-absorbing objects may be dramatically increased—something indistinguishable in a contact image (where $z = 0$) can be now strongly delineated. This delineation is in the form of a single bright/dark fringe appearing at the interface between low and high-density material.

The acquired multiple angular-dependent edge-enhanced projections may be directly used for input into tomographic reconstruction algorithms (e.g. standard filtered back-projection), obtaining corresponding edge-contrast in the tomographic slices. In the small-z approximation, known as the near-field (a small z can be determined from the Fresnel number $n_F \equiv d^2/\lambda z \gg 1$ where d is the length scale of interest and λ the x-ray wavelength) the intensity is linearly related to the 2nd transverse derivative of the phase at the exit-plane of the object [9]. However, these 'raw' reconstructions of phase contrast images can exhibit phase artefacts, often in the form of tangential streaks, caused by the sharp gradients of these edges, a type of angular under-sampling [10]. Also, and perhaps of greater importance, whilst the edge contrast may be sufficient for manual segmentation and tracing methods, any type of automatic segmentation may be quite challenging.

By applying phase retrieval as an intermediate step, tomographic slice contrast and segmentation may be dramatically improved. By inverting the phase contrast, one is able to obtain images similar to an absorption image with considerably improved signal-to-noise ratio (SNR). The form of contrast reverts from edge contrast to area contrast, from the Laplacian of the phase to a direct linear function of the phase. Various types of phase retrieval algorithms exist, both analytical and iterative (or a mix of the two) [11]. Employing only one distance and energy, single-image phase retrieval schemes such as those based on the TIE (Transport of Intensity) [12] equation are here ideal. This is particularly true in the case of dynamic sample conditions. The non-iterative algorithm by Paganin *et al.* [13] is well recognised to be highly practical in terms of its simplicity, computational efficiency and robustness. As such it has been proven useful in many applications of x-ray phase contrast imaging. This is illustrated by its selection for the basis of java-based x-ray phase retrieval software ANKA*phase* [14] (freely available as a plugin to the popular Image J package [15]).

The robustness of the algorithm is in part due to the essential nature of the algorithm as a low-pass filter. The inverse Laplacian $1/k^2$ parameter acts practically to provide a cut-off frequency beyond which the smaller spatial features are smoothed out.

Under the conditions of its derivation, describing the phase retrieval of a weakly-diffracting homogeneous object illuminated with planar monochromatic radiation (or a point-source given the addition of a simple magnification term), the algorithm may be used to accurately quantify the projected thickness of the object. The retrieved thickness map, or phase map which under these conditions may be assumed directly proportional to the former, exhibits a typical blurring. This is induced by the finite source size and detector resolution together with the fundamental assumption of the algorithm that the sample-detector distance is sufficiently small such that only a single Fresnel diffraction fringe is present in the image.

In fact the algorithm performs quite tolerably under a range of relaxed conditions. These are well known and noted for example in [14]. Indeed, in many cases of its use and particularly for the phase retrieval step in tomography, the approximation of a single-material system is no longer met. At this point the relative grey-scale values of the retrieved map may

#221629 - $15.00 USD Received 25 Aug 2014; revised 13 Oct 2014; accepted 14 Oct 2014; published 27 Oct 2014

no longer be considered quantitatively accurate. Additionally, the reconstructions are notably characterized by either an under- or over-smoothing of those material interfaces which are not the assumed single-material-to-air interface. Thus pure quantitative analysis is not possible and these maps should not be used to determine the electron density. Nevertheless, where a multi-material sample exists with several composite materials of different but not dramatically varying phase-shifting and attenuating behavior, the resulting tomogram quality may be more than sufficient for some desired form of automatic segmentation. In [16] and [17] this effect is discussed in detail, together with a variant of the original Paganin algorithm presented which may take into account multiple materials, given sufficient *a priori* knowledge of the sample. These may then be spliced together, if somewhat labor-intensively, for a final reconstruction. In their later paper, bio-medical experiments are presented where this was usefully applied and where it was deemed sufficient to use the original single-material algorithm.

We return to the main point then that use of the algorithm can be a very beneficial step in the analysis of propagation-based phase contrast tomographic data, but will in general cause a decrease in spatial resolution. Artificially tuning the single-material index of refraction input value, which in some sense may be considered to counter-effect the point-spread function (PSF) of the detector system, can temper this effect to some degree. However, this artificial tuning will add to the non-quantitativeness and lead to a general loss of area contrast. In this way one must reach a compromise between contrast and resolution.

In this paper we present and discuss one potential answer to this problem, in the form of a simple image fusion technique. This simple method works by merging, in the Fourier space, the phase contrast images before and after phase retrieval— taking just the high frequency components of the phase contrast images, which conserve the spatial resolution, and adding them via a weighted factor back into the phase retrieved result. In essence this is just putting back a small but controlled amount of the edge enhancement (and noise). The idea of retaining some component of the defocused (raw phase contrast) image in the final retrieved function, in order to compensate for deblurring effects of the imaging system such as the PSF, is discussed in [18].

Image fusion –type methods have been successfully used in 2-D with grating-based phase contrast in the application of mammography, where the three information modes of absorption, phase and dark-field (scattering) are combined in one single image to present the information easily to the radiologist. This has been done in Fourier space [19] and via wavelet component addition [20].

The easy tunability of the method proposed herein, as an additional step to the use of the TIE-based method [13] should be highlighted. The image ‘fusion’ tends to tip the method into one of image processing, and in effect may be compared to the 2D digital filtering techniques of unsharp masking and Laplacian filtering [21]. The original phase retrieval algorithm is, as stated, already used to great benefit and often not strictly quantitatively. Applications of this fusion method are limited to cases where the original single-image algorithm would already be considered. It is able to offer such a user an additional degree of choice over the key image parameters of area contrast and resolution for their segmentation. This in turn may give an extra level of control over experimental design including propagation distance, where noise *vs*. contrast can be one of the key deciding factors. One may consider it an alternative to other single image phase retrieval methods such as contrast transfer function (CTF)-based algorithms (*e.g.*, [22]) (valid in both the near- and intermediate-field) which may be more computationally difficult, still based on similar or more restrictive sample approximations and may be much less stable with respect to noise. Keeping in mind the simplicity and potential for dynamic scanning, the technique here may well be considered a useful complement to alternative quantitative techniques such as in-line holography or grating-based interferometry.

#221629 - $15.00 USD Received 25 Aug 2014; revised 13 Oct 2014; accepted 14 Oct 2014; published 27 Oct 2014

2. Theory and Experimental Layout

For any given material of complex refractive index $n_j = 1 - \delta_j + i\beta_j$ where refraction is sufficiently weak such that the x-ray wavefield matter interaction may be expressed by the projection approximation for attenuation and phase modulation (assuming paraxial incident wavefront), a sample composed of a single material gives for the phase change $\Delta\phi$:

$$\Delta\phi = -k\int_0^z \delta dz = -k\delta T(x,y) \ , \tag{1}$$

$$\text{and for the intensity transmission,} \quad I/I_0 = \exp(-\int_0^z \mu dz) = \exp\left(-\mu T(x,y)\right), \tag{2}$$

where *T(x,y)* is the projected thickness of the material along the optical (*z-)* axis, and $\mu = 2k\beta$ is the linear attenuation coefficient. Here k is the standard scalar wavevector $2\pi/\lambda$, δ is the energy-dependent phase decrement for material j, with β its corresponding absorption component.

Given a measurement of the intensity I of the modulated wavefield some small distance z downstream of the sample, with propagation effects following the conservation of optical energy known as the TIE [12], the projected thickness may be uniquely recovered as [13]:

$$T(x,y) = -\frac{1}{\mu}\ln\left(\mathcal{F}^{-1}\left\{\frac{1}{(\delta/\mu)z(k_x^{\ 2}+k_y^{\ 2})+1}\mathcal{F}\left\{\frac{I(x,y)}{I_0(x,y)}\right\}\right\}\right), \tag{3}$$

where $\mathcal{F}$ and $\mathcal{F}^{-1}$ represent the forward and inverse Fourier Transform, k_x and k_y describe the spatial frequency coordinates of Fourier space in the transverse plane dual to real space coordinates x and y.

The low-pass filter effect of Eq. (3) is attributable to the $1 / (\alpha k^2 + 1)$ term (where $\alpha \equiv \delta z/\mu$), representing the double integration step reversing the forward description of phase contrast as a linear function of the Laplacian (∇^2) of the phase. This term gives the algorithm its stability and robust behavior but also determines an effective cut-off frequency limiting the highest spatial frequencies ultimately present in the reconstructed image.

For a more meaningful value in tomography we can calculate the 2D phase map which is proportional to the retrieved term (using Eq. (1)). Tomographic reconstruction of the 3-dimensional phase of the object is possible using standard reconstruction algorithms such as Filtered Back Projection (FBP) [10] or similar.

A conventional x-ray tomographic reconstruction takes a set of angular projections containing absorption contrast to obtain the 3D distribution of μ within the sample. A set of projections containing both absorption and phase contrast could be reconstructed following the exact same steps to obtain a 3D distribution of a combination of μ plus the second derivative of the phase, the latter of which is seen as edge-enhancement [23].

Tomographic reconstruction following phase retrieval with Eqs. (3) and (1) to give the 3D phase distribution, for single-material samples with weak absorption yields a result that is theoretically directionally proportional to a traditional reconstruction of μ (equivalent to z = 0 in Eq. (3)), since δ/μ is assumed constant across the sample. Practically, as previously mentioned, the traditional absorption contrast measurement suffers from poor SNR, and visibility of structure is achieved via phase contrast edge enhancement. The phase retrieved reconstruction yields high area contrast (CNR) yet undergoes a blurring of features according to the loss of spatial frequencies determined by the magnitude of filter coefficient α.

The simple idea that constitutes the basis of this paper is to qualitatively combine the properties of the quantities tomographically reconstructed with and without phase retrieval. In

#221629 - $15.00 USD Received 25 Aug 2014; revised 13 Oct 2014; accepted 14 Oct 2014; published 27 Oct 2014

this way it is possible to keep a high CNR yet regain some easily tunable amount of the spatial frequencies otherwise lost.

The approach taken here is to apply a merging in Fourier space of the two quantities, as may be represented by the equation:

$$\text{result} = B_{\max} \mathcal{F}^{-1} \left\{ Wf(k_r, M) \mathcal{F}\left\{ A / A_{\max} \right\} + \mathcal{F}\left\{ B / B_{\max} \right\} \right\}. \quad (4)$$

Here A/A_{max} and B/B_{max} are normalized functions of the raw phase contrast image and the phase-retrieved image, respectively. k_r denotes the radial spatial frequency coordinates which correspond to the relevant image plane (e.g. the *xz*- plane when merging cross-sectional tomograms). The smooth filter (real) function, $f(k_r,M)$, is essentially a smoothed radial masking function of value zero at the zeroth frequency and rising asymptotically to 1.0 at some width M. (A non-sharp cut-off is important in order to prevent the occurrence of ringing artefacts in the inverse transform.) One example of such a function is $f = ½ [1 + erf(k_r - M)]$, where $erf(k_r)$ is the Gauss error function. W is a real weighting number, $0 < W < 1$.

It is equally possible to conduct this Fourier merging step at the level of the projections (setting k_r to the *xy*- plane) as with the reconstructed slices, of which the slight difference in effects will be later discussed. However, for sheer convenience when judging the efficacy of the method it may be preferable to work with slices, so that a new tomographic reconstruction is not required after each tweak of values (while merged projections directly viewed can be difficult to interpret).

There is also of course the possibility to combine the two image sets in another domain; for example, we were able to produce similar results using wavelet-based merging instead (not shown). The use of Fourier methods here is justified by their simplicity and consistency with FFT use of the original phase retrieval.

The pre-normalization may be carried out with respect to pixel values within a desired region, or the DC terms (image mean), but the scaling should be kept constant over the image set. The final result should possess the same mean values as the phase retrieved set, but with an extended greyscale histogram corresponding to the added higher spatial frequencies.

In essence the merging is then tunable with two parameters: the width M of the filter function and the weighting number W. The width in pixels should be scaled to the effective resolution of the optics used, but will generally be small, needing primarily to cut out the DC term of the absorption/non-phase retrieved image, and mean attenuation of those structures considerably larger than their fringe width. The weighting number may be varied much more considerably, and will generally be chosen proportional to the SNR of acquisition.

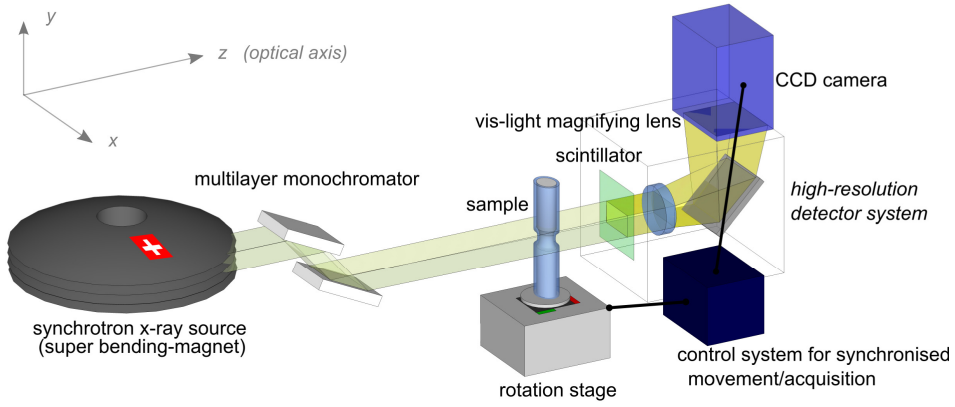

Fig. 1. Schematic detailing the setup for high resolution in-line phase contrast tomography at TOMCAT (SLS)

Experiments were conducted at the TOMCAT beamline [24] (Tomographic Microscopy and Coherent rAdiology experimenTs, Swiss Light Source, Paul Scherrer Institut,

#221629 - $15.00 USD Received 25 Aug 2014; revised 13 Oct 2014; accepted 14 Oct 2014; published 27 Oct 2014

Switzerland) shown schematically in Fig. 1, which features super-bend source and double-crystal multilayer monochromator capable of selecting energies from 8 to 45 keV with a bandwidth of 2%. It may also be operated in white-beam mode (yielding a flux of the order of 10^{14} photons/s/mm). The results shown in this section were obtained on the standard tomography endstation, consisting of an Optique Peter (Lyon, France) x-ray microscope (x-ray to visible light convertion with a 20 µm LuAG:Ce scintillator) coupled to a PCO 2000 CCD camera (7.4 µm native pixel size). With a 10x magnifying lens, the spatial resolution of the imaging system (in 2D) is less than 2 µm, or around 1 µm with 20x magnification.

The first sample imaged is an Al/SiC composite, comprising a network of SiC sheaths wrapped around a graphite core, in an Al matrix. Example values of δ and β for the composite materials at 30keV [25] are shown in Table 1. Note the attenuating properties of SiC and Al are very similar (depending on the density of the SiC sheath).

Table 1. Approximate δ and β values of the alloy composite materials at 30keV [25].

	$SiC_{(outer\ sheath)}$	$SiC_{(inner\ sheath)}$	Al	C
δ	7.4×10^{-7}	5.9×10^{-7}	6.0×10^{-7}	5.1×10^{-7}
β	1.0×10^{-9}	8.3×10^{-10}	8.9×10^{-10}	1.6×10^{-10}

2001 phase contrast projections were acquired with 1.1s exposure at 30keV and a propagation distance of 40 mm. Exposure time was chosen such that the 14-bit CCD camera chip was almost filled in the absence of sample. Reconstructions from projection to tomographic slices were performed on the TOMCAT cluster [26] using the GridRec algorithm [27],[28] and Parzen filter [29]. For the phase retrieval step, values were chosen corresponding to Al from Table 1.

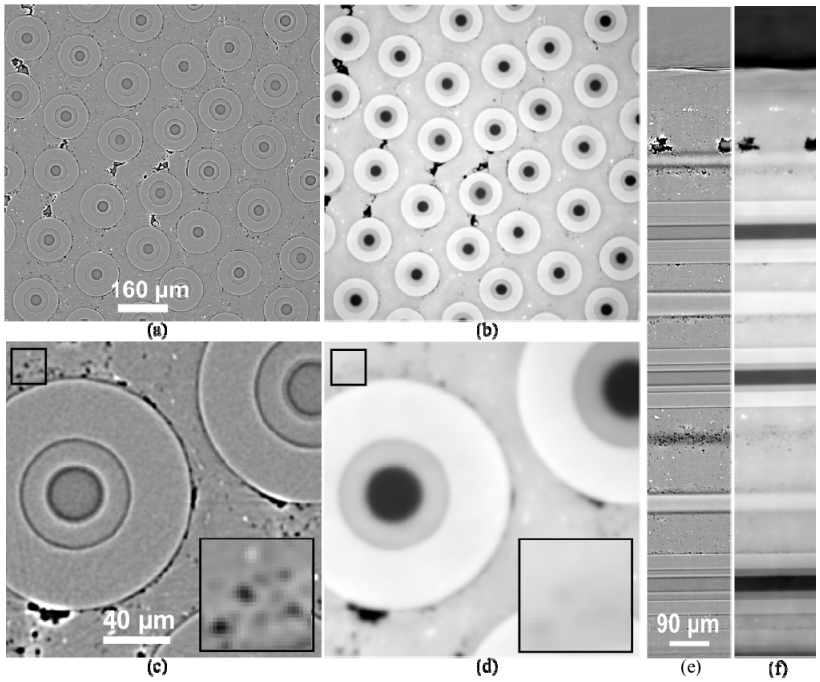

Fig. 2. SiC fiber composite sample a) raw phase contrast slice at 30keV, 40mm propagation, b) same slice as (a), reconstructed after phase retrieval of projections, c) magnified portion of (a), d) magnified portion of b). e) portion of a vertical cut-through of the standard reconstructed volume, f) equivalent portion after phase retrieval.

Figure 2 compares the cross-sectional tomographic slices of the sample applying standard reconstruction (as though assuming normal radiography projections) from raw phase contrast

#221629 - $15.00 USD Received 25 Aug 2014; revised 13 Oct 2014; accepted 14 Oct 2014; published 27 Oct 2014

images and with reconstruction of the phase after applying phase retrieval using Eq. (3) as an intermediate step. The darker values correspond to the lighter materials.

The reconstructions from the raw phase contrast projections (calculated as though maps of μ_l) appear quite sharp, but as expected with very little contrast between the Al and SiC, some between the C core and its surrounding SiC sheath, and a little more between the Al matrix and its pores (seen as dark holes). Edge enhancement is clear, especially the lighter pixels at the interfaces from higher to lower electron density, as the fringe maxima. The increased area contrast afforded by the intermediate step of phase retrieval applied to the data (here the map represents the phase) is very clear to the eye in the 2nd slice set, in particular the white-grey contrast between the outer, denser SiC sheath and the surrounding Al. Automated material segmentation of such a sample is made much easier in the phase retrieved images. Also apparent however is the loss of resolution — small features such as the tiniest pores visible within the Al matrix in the slices without phase retrieval, have become blurred.

If we consider the spatial frequencies present in the reconstructions from raw phase contrast images and those after phase retrieval, we can see the expected transition from predominantly high to predominantly low frequencies (accompanying edge contrast changing to smoothed area contrast). This is illustrated in Figs. 3a and b with the modulus of the 2D Fourier transform of the images (after a hanning windowing). Figure 3c shows the result of a weighted merging of the two according to Eq. (4). A width of 10 pixels was applied and 50% of the normalized high frequency component was added to the phase retrieval image. These are represented more quantitatively through an azimuthally-averaged plot of the radial frequencies in Fig. 3d.

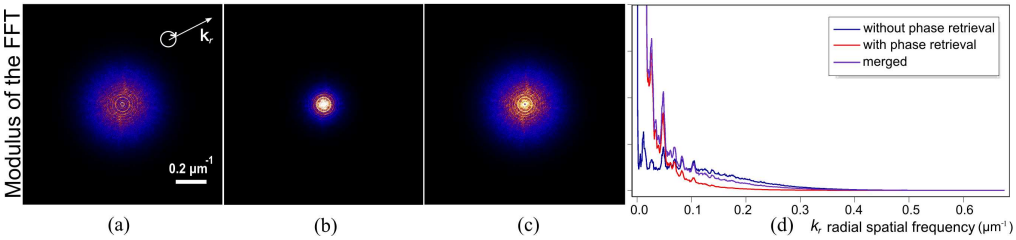

Fig. 3. Modulus of the 2-D Fourier Transform: a) standard slice reconstruction b) slice after phase retrieval of projections, c) merged. A logarithmic colour-map is used for illustrative purposes. In d) the azimuthally-averaged plot of a, b and c is shown.

Figure 4 then shows the final merged equivalent to the pre- and post-phase retrieval tomographic regions of Fig. 2. In the larger FOV, the difference between phase retrieval and merged result is not visually apparent. Upon closer inspection of a zoomed-in region however, the increased spatial resolution becomes clear. Those small porous features which are blurred out in Fig. 4e are significantly more distinct in Fig. 4f, yet without the obvious bright fringes of Fig. 4d.

#221629 - $15.00 USD Received 25 Aug 2014; revised 13 Oct 2014; accepted 14 Oct 2014; published 27 Oct 2014

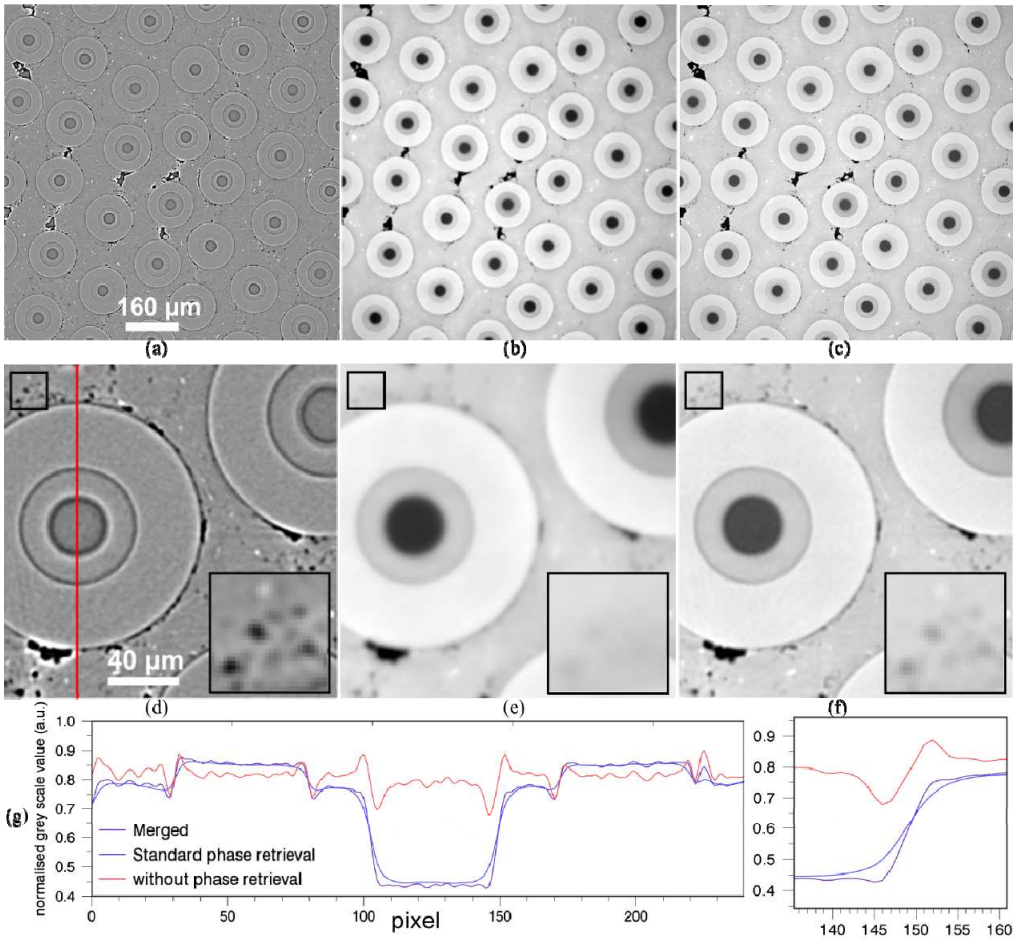

Fig. 4. SiC fiber composite sample a) standard slice reconstruction b) slice after phase retrieval of projections, c) slice containing merged information from slices a) and b). d,e,f: zoomed in regions. g) line profiles cut from the fibers of d-f.

For a more quantitative comparison of these 3 tomographic sets, we can look at the line profiles of each, cut-through one composite fiber, shown in Fig. 4g. Again this shows clearly the increased CNR yielded by the phase retrieval (blue compared to the raw reconstruction shown in red). The purple profile of the merged reconstruction is essentially just the blue plus a damped amount of the edges of the red "added back in". Correspondingly some noise is also put back into the image.

The profiles here describe a typical behavior of the phase retrieval algorithm when applied to a sample of multiple materials of similar but non-identical refractive indices. Note the non-flat (curving sloped) steps of the different materials. This comes from the application of the filter strictly designed for a single interface-type (e. g. material A to air). When two fringe sets corresponding to two different interface types are smoothed, the effect is not equal resulting in the slope between the two interface points. Although a 'ground truth' map of the phase of this sample is not known, computational simulations (not shown) of a similar model with flat step functions of density show the same behavior.

Finally, to show the versatility of this simple method of Fourier merging, we move from materials science to a new example from botany. A second sample, this time of a *Spartina Cortina* leaf was tomographically scanned in a similar setup to that of the composite fiber.

#221629 - $15.00 USD Received 25 Aug 2014; revised 13 Oct 2014; accepted 14 Oct 2014; published 27 Oct 2014

Here the 20x lens was employed giving a 0.37 μm effective pixel size. 1001 projections of 250 ms exposure each were acquired at 12keV. This plant is from the wetlands and the experiment aim was to visualize exchange of CO_2 and O_2 in the plants whilst submerged in water. The fresh samples were encased in small plastic capillary tubes filled with water and the setup was designed for maximal possible absorption contrast. Whilst the roots of the plant exhibited good absorption contrast, the thin leaves of the plant gave little, and at the same time the distance from sample to the detector (including within the water-filled tube) provided enough propagation of the x-rays to give significant edge-enhancement of the air-water and air-plant tissue interfaces. Thus it proved a good candidate for phase retrieval: we used δ and β values of 1.60 x10^{-6} and 2.40 x10^{-9} corresponding to H_2O at 12keV [25] for a *z* of 12mm.

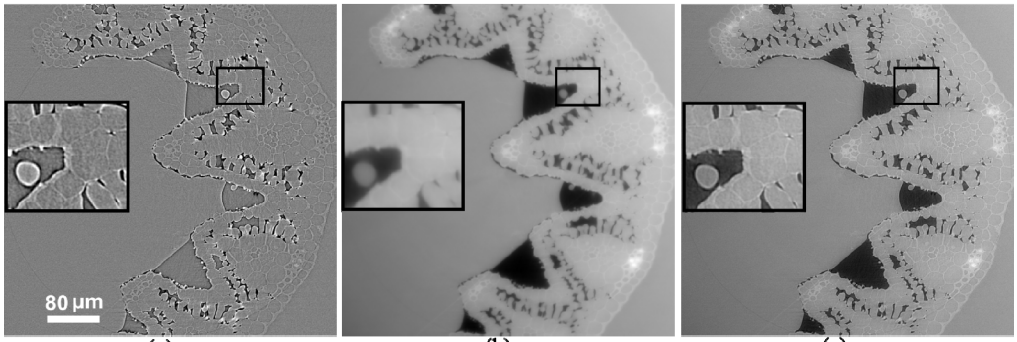

Fig. 5. *Spartina* sample a) standard slice reconstruction b) slice after phase retrieval of projections, c) slice containing merged information from slices a) and b). Magnified regions inset.

These results are shown in Figs. 5a-c. The phase retrieval clearly inverts the bright-dark fringes of the air-water interfaces in the leaf and yields strong area contrast in its place. A blurring effect may be seen at the same time, however, which is reduced in the merged image of Fig. 5c, where a weighting of 50% of the higher spatial frequencies was again used.

3. Discussion

We evaluated the performance of the technique with measurements of the two metrics: the area Contrast-to-Noise Ratio (CNR) and spatial resolution (SR). Here we use for the definition of CNR the following expression:

$$CNR = \frac{\overline{S}_1 - \overline{S}_2}{\sqrt{\sigma_1^{\,2} + \sigma_2^{\,2}}}, \tag{5}$$

where S_1 and S_2 refer to the mean intensity (signal) values for two regions of interest (i.e., different materials) and σ_1 and σ_2 denote the standard deviation of those respective regions (indicating the noise levels).

Typical spatial resolution measurements are based on threshold minima (with respect to the noise level) of the spatial frequencies of the image. A simple method is to compute the Fourier Transform (the square of the absolute value of the intensity FT yields the spectral power). A measurement of the frequency at which the power drops to twice that of the noise baseline gives one measure of the spatial resolution (as the length scale corresponding to the inverse of the frequency), see e.g. [30].

Table 2 displays the CNR values calculated for the SiC composite sample, for the three adjacent materials: Al matrix to outer SiC sheath, outer SiC sheath to inner SiC sheath, and inner SiC to C core.

#221629 - $15.00 USD Received 25 Aug 2014; revised 13 Oct 2014; accepted 14 Oct 2014; published 27 Oct 2014

Table 2. Comparison of area contrast-to-noise values for different material pairs. The * denotes a number which is higher than expected, but can be attributable to behavior of the original algorithm when applied to multi-materials.

	CNR		
	Al-SiC$_{(outer)}$	**SiC$_{(outer)}$-SiC$_{(inner)}$**	**SiC$_{(inner)}$-C**
without phase retrieval	0.1	0.2	2.6
with phase retrieval	6	7	27
with 50% merging	4	6	31*

With a sample such as this, useful CNR values should be calculated over reasonably sized regions of interest centered as much as possible between interfaces. These regions are assumed homogenous for the purposes of the calculation. Any sloped curvature of the phase retrieval approximation near interfaces will add to the variance of the data, which is indiscriminately attributed to the noise component of the CNR. Selection of vertical regions along the axis of symmetry of the fibers is the best way to achieve near-homogeneity in our case. However, the merged phase retrieval value of 31 in Table 2 is higher than the un-merged value of 27, presumably because the latter was still underestimated due to its curvature over the region and the resulting inflated variance.

Table 3 presents the spatial resolution of the sample, calculated over the whole slice. From these two tables it can be observed that the 50% merged reconstructed image has a useful balance of the properties of the reconstructions with and without phase retrieval. The resolution is approximately half way between the limiting lower resolution of the phase retrieval, and the upper resolution of the non-phase retrieved data. The contrast is still much closer to that of the phase retrieved data.

Table 3. The resolution of SiC composite.

	resolution
without phase retrieval	1.86 μm
with phase retrieval	2.57 μm
with 50% merging	2.24 μm

Table 4 displays the CNR of the water-air interface, and the resolution of the whole tomogram of the *Spartina* leaf sample. Once again, the 50% merged image manages to retain a CNR that is close to the upper limit of the phase retrieved CNR, but at a reduced resolution.

Table 4. CNR of water-air interface and resolution of *Spartina* leaf sample.

	CNR water-air	**resolution**
Without phase retrieval	0.6	0.88 μm
with phase retrieval	30	1.1 μm
with 50% merging	27	1.04 μm

As we have discussed, the strength of the filtering present in the original phase retrieval step, given by α, is responsible for the known gain in CNR at the cost of resolution.

Instead of the merging, the alpha term in the phase retrieval may also be varied to produce sharper images (a form of 'software tuning') but only to a certain degree, as this will also adversely affect the area contrast. If a significant degree of the higher frequencies is to be regained, the merging method is a preferable, more controllable way of keeping these frequencies without affecting the contrast as much. See Fig. 6.

#221629 - $15.00 USD Received 25 Aug 2014; revised 13 Oct 2014; accepted 14 Oct 2014; published 27 Oct 2014

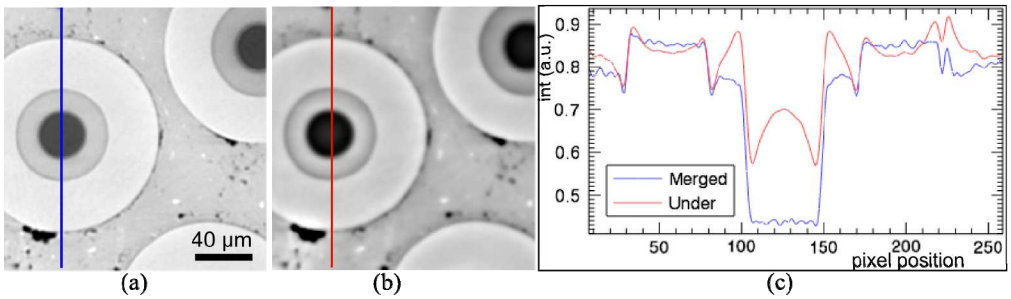

Fig. 6. Comparison of equivalent-region slices of the SiC fiber composite sample with a similar spatial resolution, obtained in two different ways: a) slice containing phase retrieval with 50% higher frequencies merged, and b) slice reconstructed directly after phase retrieval using a 'tuned' filter coefficient $\alpha=\delta z/\mu$ reduced by a factor of 5. c) overlay of the two profiles, where the undersmoothing of interfaces from the reduced coefficient give an undesirable curvature across each material.

Choice of the merging factors, most specifically the weighting factor for the high frequency components, is best determined by the needs of the user. In most cases they are seeking (hopefully automated) segmentable tomograms at an acceptable resolution. In a quick trial-and-error process conducted by the user, merged tomograms may be generated with various weightings and run through their chosen segmentation software. We have seen that segmentation based on threshholding plus some growing algorithm prefers a moderately low weighting factor, yielding images less sharp than that which would be picked by eye alone. The degree of grey-scale separation will of course be sample dependent. For future development users with consistent applications could consider the use of maximum likelihood optimization methods to automatically refine their parameter choice.

As previously stated, the use of this fusion method is best suited to cases where the original phase retrieval algorithm is deemed suitable. I.e., the sample should be either composed of homogeneous material (may be porous etc., in which case the phase retrieval parameters will be matched to the material/air interface), or of materials with similar δ/β ratios. It should not be required that the reconstructions be strictly quantitative. The original algorithm is also useful in that the object does not need to be a phase object—the approximation allows weak absorption. The presence of heavier, more absorbing objects amongst the desired structures can lead to 'contamination' of the images as the values 'bleed' into adjacent areas after the phase retrieval from over-smoothing (see measures in [16]- [17]). For this reason higher x-ray energies may be advisable as the linear attenuation coefficient drops faster with increasing energy than the phase decrement. Without losing too much phase contrast, the relative difference in δ/β values of the different composite materials can be decreased. This can help to reduce the aforementioned under- and over-smoothing of interfaces that are not so well matched to the input material parameters chosen.

As previously mentioned, single-image methods of phase retrieval are particularly useful when the sample conditions are dynamic- in many cases the experimenter may be attempting to reduce the tomographic scan times as much as possible. As well as only measuring at one distance, a limited number of projections may be used, and/or short exposure times. White or polychromatic beam, with the associated increase in photon flux could also be a valid option. As propagation-based phase contrast is relatively insensitive to the effects of temporal coherence [7], the phase retrieval is also applicable [14], where the input parameters may be matched to the peak x-ray energy. The result is a somewhat reduced contrast and resolution depending on the bandwidth (but this tradeoff may still be preferable if it delivers the required scan time). The image merging is equally applicable to white beam usage, in order to regain some resolution.

#221629 - $15.00 USD Received 25 Aug 2014; revised 13 Oct 2014; accepted 14 Oct 2014; published 27 Oct 2014

Quite commonly phase contrast experiments may be designed based first on an experimental determination of the optimum propagation distance, source energy and detector acquisition times. Whilst rules of thumb such as the Fresnel number are useful indicators a quick parameter space sweep can be invaluable. For determination of propagation-distance, use of the original phase retrieval tends to mean finding the maximum distance that keeps within the near-field regime. Up to this point the CNR rises dramatically with distance but then drops, whilst the resolution, tied to CNR also peaks at a small non-zero distance and then worsens with increased distance as the small-distance approximations break down. With the additional application of the merging technique, users with fixed resolution constraints can choose to work at a propagation-distance greater than that they might otherwise pick, yielding a CNR higher than they would otherwise achieve with a similar resolution (not using the merging). One example is shown in [31].

It is also useful to consider the cases where the merging technique does not work so well. We have mentioned the desirability of reducing the difference in δ / β values of composite materials (since most samples will not be truly homogeneous); conversely, it is not so applicable to very highly attenuating samples (although one would equivalently not need it at this point, as absorption contrast alone should be sufficient). Samples with too much phase contrast present in the non-retrieved images are also not ideal, since they often lead to phase artefacts, which, as a form of high frequency structure, will also end up back in the final merged image. For this reason it may be preferable to conduct the merging process at the level of projections, since the filter of the reconstruction (e.g shepp-logan, hamming, parzen [10]) will have a dampening effect on these. The weighting factor chosen for this will be a different value to that used with the slice-based merging. The method has also been highlighted as useful for dynamic imaging (see, *e.g.* [32]), but there will be cases where experiments must be conducted at extremely low exposure times, giving very poor SNR values of the raw phase contrast images. In such a case the fully robust smoothing of the original phase retrieval is vital for achieving sufficient CNR of the tomograms. Then, merging would involve the re-introduction of too much noise to be considered worthwhile to the final image quality.

This method is very easily incorporated into any procedure which is currently based on the original phase retrieval algorithm. It has a very low number of parameters to consider (essentially two) which are easily judged by the user.

4. Conclusions

A simple single-image method of Fourier merging images before and after phase retrieval has been demonstrated, for the 3D sharpening of the retrieved sample phase at a high contrast. This method is very easily incorporated into any procedure which is currently based on the original phase retrieval algorithm. It has a very low number of parameters to consider (essentially two) which are easily judged by the user. It is suited to a reasonable range of applications that would already be initially considering usage of the original phase retrieval algorithm, additionally offering a greater control of image quality parameter choice. As such it should be considered a useful compliment to other less robust, or more time consuming yet more uniformly quantitative methods of phase contrast-based 3D sample mapping.

Acknowledgments

This work was supported by Centre d'Imagerie BioMédicale (CIBM) of the UNIL, UNIGE, HUG, CHUV, EPFL and the Leenaards and Jeantet Foundations. We are grateful to Stuart Stock for the use of his SiC fibre sample. Special thanks also to Ole Peterson for letting us work with his plant samples. Following the conclusion of this work, the first author is now employed at Monash University in Clayton, Australia.